Consistent hierarchies of single-neuron timescales in mice, macaques and humans

Authors: Zachary R. Zeisler[1], Marques Love[1], Ueli Rutishauser[2,3,4,5], Frederic M. Stoll[1†], and Peter H. Rudebeck[1†*]

Author affiliations:

1. Nash Family Department of Neuroscience, Lipschultz Center for Cognitive Neuroscience, and Friedman Brain Institute, Icahn School of Medicine at Mount Sinai, One Gustave L. Levy Place, New York, NY 10029
2. Department of Neurosurgery, Cedars-Sinai Medical Center, Los Angeles, CA 90048
3. Department of Neurology, Cedars-Sinai Medical Center, Los Angeles, CA 90048
4. Center for Neural Science and Medicine, Department of Biological Sciences, Cedars-Sinai Medical Center, Los Angeles, CA 90048
5. Division of Biology and Biological Engineering, California Institute of Technology, Pasadena, CA 91125

[†] Denotes equal contribution

[*] Corresponding author

Correspondence should be addressed to:

Dr. Peter Rudebeck – peter.rudebeck@mssm.edu

Lipschultz Center for Cognitive Neuroscience, Nash Family Department of Neuroscience and Friedman Brain Institute

Icahn School of Medicine at Mount Sinai

One Gustave L. Levy Place

New York, NY 10029

Word Count:

Abstract: 161 words

Main Text: 3858 words

Figures: 3 (plus 1 supplemental)

Tables: 2 (in methods)

1 Abstract

2 The intrinsic timescales of single neurons are thought to be hierarchically organized across the
3 cortex. This conclusion, however, is primarily based on analyses of neural responses from
4 macaques. Whether hierarchical variation in timescales is a general brain organizing principle
5 across mammals remains unclear. Here we took a cross-species approach and estimated
6 neuronal timescales of thousands of single neurons recorded across multiple areas in mice,
7 monkeys, and humans using a task-agnostic method. We identify largely consistent hierarchies
8 of timescales in frontal and limbic regions across species: hippocampus had the shortest
9 timescale whereas anterior cingulate cortex had the longest. Within this scheme, variability
10 across species was found, most notably in amygdala and orbitofrontal cortex. We show that
11 variation in timescales is not simply related to differences in spiking statistics nor the result of
12 cytoarchitectonic features such as cortical granularity. Thus, hierarchically organized timescales
13 are a consistent organizing principle across species and appear to be related to a combination of
14 intrinsic and extrinsic factors.
15

16 Highlights

17

18 • Similar hierarchies of single neuron timescales exist across humans, macaques, and mice
19 • Humans diverge from an otherwise conserved hierarchy in amygdala and OFC
20 • Timescale variability in ventral frontal cortex is not entirely related to cytoarchitecture

21

Introduction:

Receptive fields are a foundational concept in psychophysics and neuroscience, a classic example being the spatial receptive fields of single neurons in primary visual cortex (Hubel and Wiesel, 1962; Spillmann, 2014) and higher-order parietal and frontal areas (Viswanathan and Nieder, 2017). An influential line of work has extended this framework to the temporal domain (Murray et al., 2014). Using the rate of exponential decay of the spike-count autocorrelation, Murray and colleagues extracted the intrinsic temporal receptive field, or timescale, of a single neuron or population of neurons. These neural timescales, which are hypothesized to reflect the amount of time over which a neuron integrates information, appear to be hierarchically organized across the brain (Murray et al., 2014; Nougaret et al., 2021). Neurons within sensory cortex have shorter timescales, while neurons within higher-order associative areas, particularly in frontal cortex, have longer timescales. Convergent evidence from fMRI in humans (Hasson et al., 2008; Honey et al., 2012; Raut et al., 2020), fMRI and neurophysiology recordings in non-human primates (Murray et al., 2014; Manea et al., 2022, 2024), and modelling work (Gao et al., 2020; Perez-Nieves et al., 2021; Fontanier et al., 2022; Li and Wang, 2022) suggest that this hierarchical organization of timescales may be a fundamental principle of brain organization. Despite this, analyses of single neuron timescales across humans and animal models utilizing the same data modality and fitting procedure have been lacking. This is a key consideration given the differences in temporal resolution between fMRI and single neuron activity.

Neural timescales are hypothesized to be driven by the physical properties as well as connectivity of single neurons (Soltani et al., 2021). The divergence in brain anatomy across humans, non-human primates, and rodents suggests that there could be corresponding changes in timescales across brain areas that mirror anatomical differences (Cavanagh et al., 2020). For instance, the dorsal portion of anterior cingulate cortex (ACC) is largely conserved across humans, macaques and mice as it is agranular cortex (Wise, 2008; van Heukelum et al., 2020). While the timescales of ACC neurons across primate and rodent species have not been directly compared, their shared anatomy suggests that they may be similar. By contrast,

50 amygdala, an area which sends strong projections to ACC and other frontal cortex areas

51 (Ghashghaei et al., 2007; Hintiryan et al., 2021; Zeisler et al., 2023), is markedly different across

52 humans, macaques and mice – particularly in the basolateral subdivision (Chareyron et al.,

53 2011; Zeisler et al., 2024). Whether these differences in amygdala anatomy are mirrored by

54 differences in timescale is unknown.

55   To address these issues, we compared the timescale of tens of thousands of neurons

56 within frontal cortex, amygdala, and hippocampus of mice, macaque monkeys, and humans.

57 We identified largely consistent hierarchies across species within this amygdala-hippocampus-

58 frontal cortex system, with key exceptions particularly in amygdala. Importantly, divergences

59 from the common hierarchy were not related to known differences in frontal cortex

60 cytoarchitecture.

61 ## Results

62   We analyzed the firing activity of 17,458 single neurons recorded in orbitofrontal cortex

63 (OFC), medial prefrontal cortex (mPFC), anterior cingulate cortex (ACC), amygdala and

64 hippocampus in three species: humans, macaque monkeys, and mice (**Figure 1A**, **Table 1,** see

65 **Methods** for detailed explanation on anatomical mapping). Multiple methods have been put

66 forth to calculate the temporal timescales of single neurons. Timescale estimation originally

67 relied only on the spiking activity during periods in which animals were not actively performing

68 a task but rather sitting in restful attentiveness (Murray et al., 2014). While well-suited for

69 analysis of data recorded from non-human primates, who often perform tasks with rigid

70 temporal structure, such an approach is not optimal for recordings from rodents or humans,

71 where tasks are often performed with more continuous and variable time courses. One method

72 based on the distribution of inter-spike intervals (ISI) allows for the estimation of timescales

73 irrespective of task events and could therefore be readily applied to the activity of neurons

74 recorded in different species (Fontanier et al., 2022). Importantly, the estimated timescales

75 from the approach that uses the ISI and the more standard approach (Murray et al., 2014) have

76   been shown to be highly correlated with one another, suggesting that they are modeling the

77   same underlying physiological properties.

78   To estimate the intrinsic timescale of each of the neurons we analyzed, we employed

79   this latter ISI-based method from Fontanier, Sarazin and colleagues (Fontanier et al., 2022). In

80   brief, we fit an exponential decay function to the descending portion of the distribution of ISIs

81   according to the following equation:

82
$$R(k\Delta) = A\left[e^{-(\frac{k\Delta}{\tau})} + B\right]$$

83   where $k\Delta$ is the time lag between bins, τ represents the neuron's *timescale*, describing the rate

84   of decay of the autocorrelation distribution, and A and B are free parameters which together

85   describe the peak and asymptotic limit of the autocorrelation. We also extracted the time bin at

86   which the autocorrelation begins decreasing, which we refer to as *latency*. Only neurons for

87   which the model fit well ($R^2 > 0.5$) and exhibiting timescales within the range $10 < \tau < 1000$ were

88   included for further analysis (n=13,755 single neurons, 78.7% success; **Figure 1B**).

89   Mice, macaques, and humans exhibited largely similar hierarchies of single neuron

90   timescales and latencies across areas (**Figure 1C, D**). Across all three species, ACC neurons

91   showed the longest timescales and latencies while hippocampus neurons showed the shortest

92   timescales. Other areas were characterized by greater across-species variability. Notably,

93   human amygdala neurons had a significantly shorter timescale compared to macaques and

94   mice (**Figure 1E**; middle). All three species also had different amygdala latencies. Furthermore,

95   the timescales of single neurons in OFC were statistically distinguishable in all three species,

96   with humans exhibiting the longest timescale. Taken together, we found numerous similarities

97   between the timescale and latency hierarchies across these three species, with a notable

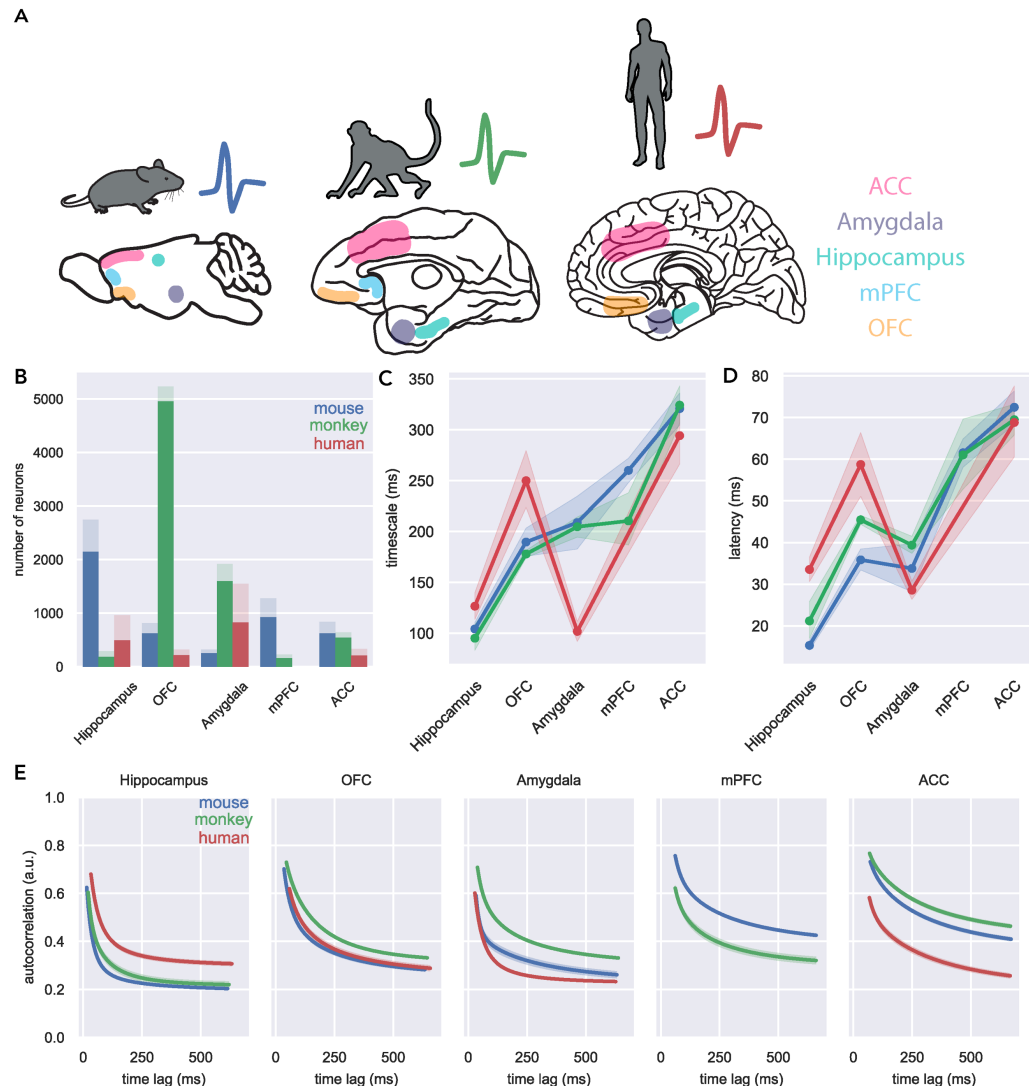98   exception for OFC and amygdala neurons in humans.

Figure 1. Single neuron timescale and latency hierarchies are largely conserved across species.
A) Schematic representing the approximate position of brain areas from which recordings were collected in mice (left), macaques (middle) and humans (right); ACC in pink, amygdala in purple, hippocampus in cyan, mPFC in light blue, OFC in orange (see **Methods** for detailed explanation of area assignments). B) Number of neurons considered (light colors) and successfully fit (dark colors) across all brain areas. C) Average [±95% CI] timescales and D) latencies for each area in humans (red), macaques (green) and mice (blue). There was a main effect of both species ($F_{(2)}$ = 48.37, p = $1.2*10^{-21}$) and area ($F_{(4)}$ = 422.15, p = 0) on timescale as well as a significant interaction ($F_{(8)}$ = 31.53, p = $1.7*10^{-49}$). All three species had different OFC timescales (OLS regression, mouse vs monkey: $t_{(2)}$ = 1.961, p = 0.05; monkey vs human $t_{(2)}$ = 7.332, p = $2.6*10^{-13}$), OFC latency (mouse vs monkey: $t_{(2)}$ = 5.672, p = $1.5*10^{-8}$; monkey vs human $t_{(2)}$ = 4.788, p = $1.7*10^{-6}$), and amygdala latency (mouse vs monkey: $t_{(2)}$ = 2.096, p = 0.036; monkey vs human $t_{(2)}$ = 6.379, p = $2.1*10^{-10}$). Human amygdala timescale was different from the other species (mouse vs monkey $t_{(2)}$ = 0.338, p = 0.735; monkey vs human $t_{(2)}$ = 13.331, p = $2.6*10^{-39}$). E) Average fits for neurons from each area and species. Lines are plotted by the mean fit parameters from successfully fit neurons, with shading indicating the standard error.

99

100   While the above analyses focused on the average timescales for each area and species,

101   timescales were not necessarily uniform within a given area. Indeed, we found large variability

102   in the distributions of timescale and latency within each area and across all three species

103   (**Figure 2 A, C-D**). In fact, both timescale and latency distributions across most considered areas

104   and species had unequal variances. This within-area variation is particularly prominent in ACC,

105   where mice, macaques, and humans all had a bimodal distribution of timescale: a small

106   population of neurons with short timescale and a larger population of neurons with longer

107   timescales. Such consistent heterogeneity across species within an area potentially provides

108   insight into the organizing role that timescales might play in the temporal processing of

109   information. Indeed, it could be the case that the distribution of timescales within an area is

110   more critical for supporting that area's function than the average timescale.

111   Across the different areas and species, there was also significant variability in the

112   latency measure that was fitted to each neuron's spiking activity (**Figure 1D**). Here ACC and

113   mPFC had the longest latency whereas hippocampus generally had the shortest. Further, within

114   each area there was also a high degree of variability in the latency (**Figure 2D**). Importantly,

115   while timescale and latency exhibit some degree of correlation (**Figure 2B**), each explains only

116   half of the variance in the other. This point highlights that latency is a factor that is partially

117   separable from the timescale and likely contributes to how information is temporally processed

118   within a brain area.

119   One potential issue with fitting exponential decay functions to the activity of single

120   neurons is that they might be influenced solely by the firing rates of the neurons. Thus, we next

121   checked that our timescale and latency estimates reflected distinct neuronal functional

122   properties, independent from the influence of firing rate. To that end, we built regression

123   models to predict timescales based on spiking statistics, areas and species (**Supplemental**

124   **Figure 1**). We found that the number of spikes entered into the analysis only had a significant

125   influence on a neurons' timescale while the number of spikes, mean firing rate, and Fano factor

126   all influenced the neural latencies. These parameters, however, offered little additional

127   explanatory power compared to species and area, explaining significantly less variance than

128   area and species alone. Thus, the neural timescale and latency that we reported above (**Figures**

129   **1, 2**) represent features of neuronal dynamics that are distinct from classical spiking statistics.
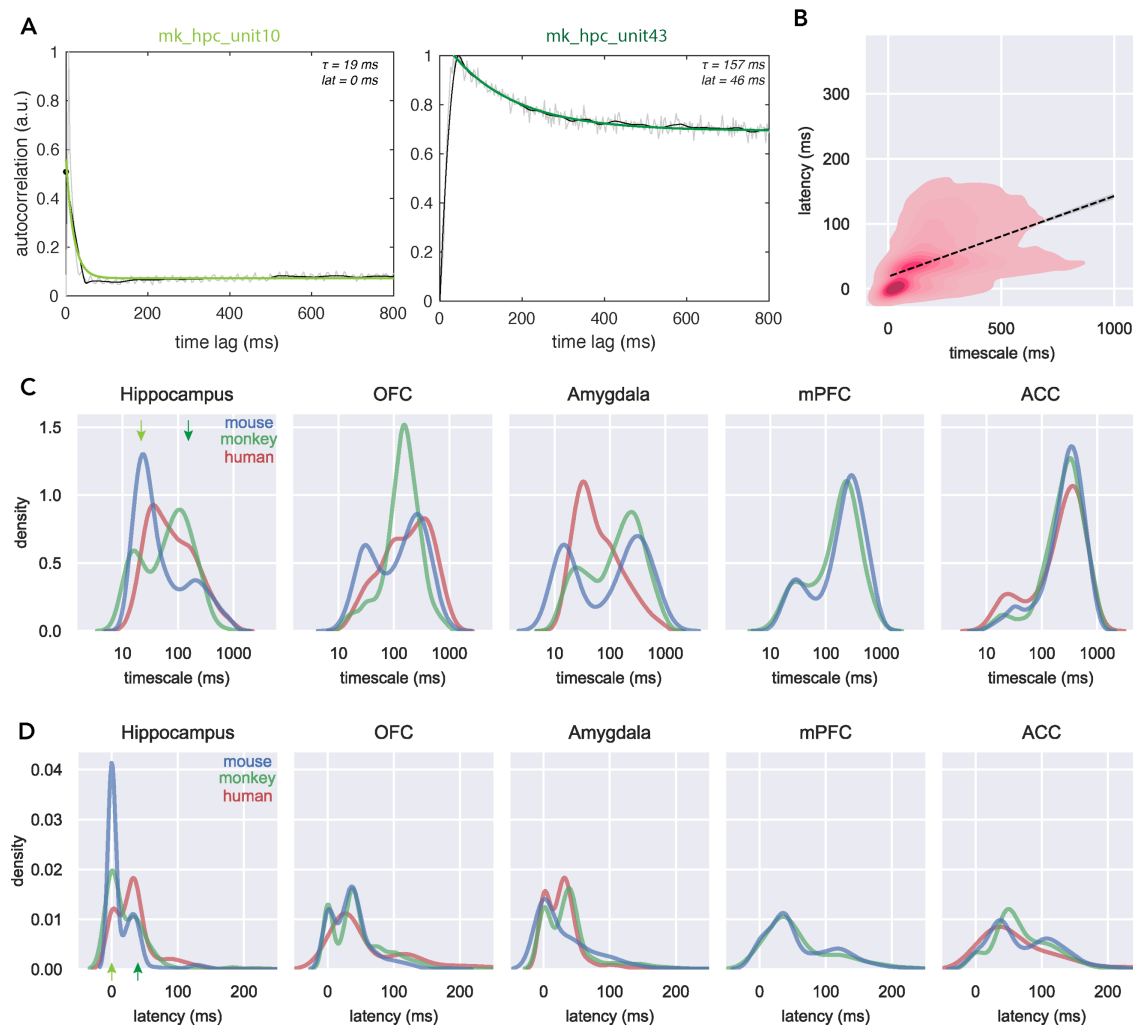
Figure 2: Distributions of timescale and latency for individual neurons. A) Two example single-neuron fits from macaque hippocampus with relatively short (left; light green) and long (right; dark green) timescales. Grey traces indicate normalized ISI distribution, the black line is the smoothed autocorrelation, and the green lines are the fit autocorrelation function, specified by timescale (τ) and latency (*lat*) shown in the top right of each panel. B) Density plot of timescale and latency, with regression line overlaid. Timescale and latency are correlated with each other (OLS regression: $R^2 = 0.501$, $p < 0.001$). C) Density histograms showing distribution of timescales across neurons recorded within each brain area. The timescales of neurons from OFC, amygdala, and mPFC all have unequal variance across species (Brown-Forsythe test: $p < 0.004$). Green arrows indicate the position of the example cells shown in panel A. D) Same as C for latencies (bottom). All areas with the exception of mPFC had unequal variance regarding latencies ($p < 10^{-6}$).

130

131   *The relationship between cytoarchitecture and timescales within ventral frontal cortex*

132   As previously noted, ACC in humans, macaques, and mice is agranular cortex (van

133   Heukelum et al., 2020). By contrast, OFC in macaques (**Figure 3A**) and humans is composed of

134   granular, dysgranular, and agranular cortex (Carmichael and Price, 1994; Wise, 2008). OFC in

135   mice, by contrast, is entirely agranular. One possibility is that these differences in granularity

136   might underlie the timescale and latency differences we observed in OFC across species (**Figure**

137   **1**). To assess this, we concentrated our analysis on recordings from 12,043 single neurons in

138   macaque ventral frontal cortex, of which 5,230 were included in the previous analyses of

139   macaque OFC in **Figures 1** and **2**. This dataset included the activity of single neurons recorded

140   using 157-channel semi-chronic microdrives in two monkeys, where each electrode trajectory

141   was precisely reconstructed (Stoll and Rudebeck, 2024b, 2024c). Using standard histological

142   techniques, the ventral frontal cortex was subdivided into 8 cytoarchitectonic areas based on

143   analysis of Nissl-, SMI-32- and calbindin-stained tissue series (**Figure 3A**). This allowed us to

144   pinpoint the precise location of recorded neurons according to previous parcellations of the

145   ventral frontal cortex of macaques (Carmichael and Price, 1994; Rapan et al., 2023). Thus, we

146   could compare the timescales of neurons from neighboring subdivisions with distinct cortical

147   granularity; fully granular areas 11m/l, 12l, 12m, and 12o, dysgranular areas 12r, 13m, and 13l

148   areas, and agranular insula (AI; the number of neurons in each subdivision is shown in **Figure 3B**

149   and **Table 2**).

150   We found that timescale variability across macaque ventral frontal cortex could not be

151   fully explained by differences in granularity (**Figure 3C,** left). While there was a main effect of

152   granularity, such that neurons in granular areas tended to exhibit longer timescales than those

153   in dysgranular areas, hierarchical model comparison indicated that granularity did not

154   significantly improve a model predicting neural timescales based on area alone. Notably,

155   adjacent areas 12m and 12r were most different from other granular and dysgranular areas,

156   respectively as they had relatively longer timescales. Neuronal latencies were found to have a

157   different relationship to granularity (**Figure 3D**, right). Specifically, granular and agranular areas

158   demonstrated longer latencies than dysgranular – and a model predicting latency with

159   granularity performed better than a model containing area alone. Thus, the presence or

160   absence of an internal granule cell layer does not appear to be a strong predictor of the

161   timescale of single neurons in an area. Granularity, however, does significantly affect neuronal

162   latency, which may be related to variation in the cortical microstructure (Gao et al., 2020).

163   Finally, we investigated whether single neuron timescales and latencies could be related

164   to the spatial location of neurons on the ventral surface of the frontal lobe. Across frontal

165   cortex there are both antero-posterior (AP) and medio-lateral (ML) gradients in the connections

166   from other parts of the brain, especially the amygdala (Ghashghaei et al., 2007) and

167   hippocampus (Aggleton et al., 2015). We hypothesized that such differences in long-range

168   inputs could drive differences in neural timescales. To this end, we assessed whether the AP

169   and ML coordinates of each recorded neuron influenced neuronal timescales and latencies. In

170   both animals, there were main effects of the AP position ($F(1) = 20.16$, $p = 7.3*10^{-6}$), ML

171   position ($F(1) = 26.97$, $p = 2.1*10^{-7}$), and a significant interaction ($F(1) = 47.12$, $p = 7.5*10^{-12}$),

172   such that timescales were longest in neurons recorded in posterior/lateral and anterior/medial

173   regions. Thus, the variation in timescales in ventral frontal cortex could be influenced by the

174   patterns of projections into the frontal cortex from limbic (Cavada et al., 2000; Ghashghaei et

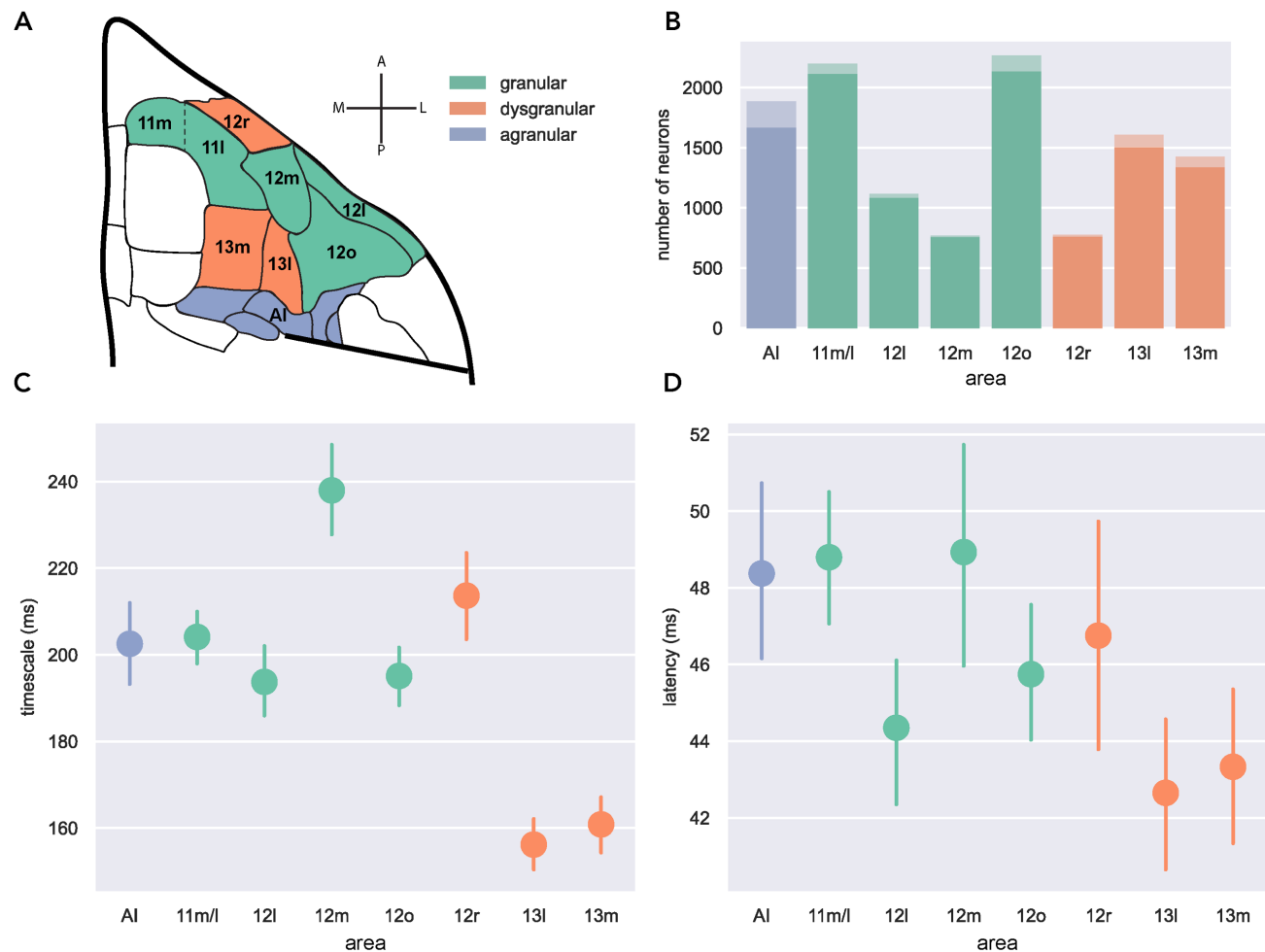175   al., 2007) and/or sensory systems (Carmichael and Price, 1996).

176

Figure 3. Timescales and latencies within macaque ventral frontal cortex are not purely driven by cortical granularity. A) Schematic representations of the orbital surface of macaque's brain showing the relative location and cytoarchitectonic subdivisions of the ventral frontal cortex included in this analysis. B) Number of recorded neurons (lighter bars) and number of neurons successfully fit (darker bars) across areas. C) Average (+/-95% confidence intervals) timescale of single neurons in granular (green), dysgranular (orange) and agranular (blue) subdivisions of ventral frontal cortex. There is a significant main effect of granularity (OLS regression, dysgranular < granular: $t(2) = 10.58$, $p = 4.7*10^{-26}$; dysgranular < agranular: $t(2) = 7.34$, $p = 2.36*10^{-13}$; agranular ≈ granular: $t(2) = .19$, $p = 0.85$); although a model which includes area and granularity is no better at predicting timescale than one which includes area alone ($F(2) = 1.36$,

Discussion:

177

178   Here, we computed the timescales of single neurons recorded in parts of the fronto-

179 limbic system in humans, macaques, and mice. We found that across the different species,

180   single-neuron timescales followed a similar hierarchical organization; hippocampus had the

181   shortest timescale whereas ACC had the longest. Further, while timescales in hippocampus,

182   ACC, and medial frontal cortex were highly consistent across species, the timescales of

183   amygdala and OFC neurons were more variable. We further found that differences in

184   timescales across macaque ventral frontal cortex followed specific spatial patterns but were

185   independent of the underlying variation in cytoarchitecture. Taken together, we report that

186   hierarchical organization of brain systems is common between three mammalian species

187   frequently studied in neuroscience, despite differences in some areas.

188   *Timescales in subcortical areas*

189   One of the most striking results from these data was the large divergence in amygdala

190   timescale across the species that we studied (**Figure 1**). We observed that mice had the longest

191   amygdala timescales while human amygdala timescales were the shortest. It is important to

192   note that within these mammals, large anatomical differences between the amygdala of

193   different species exist (Chareyron et al., 2011). Such differences in amygdala structure are most

194   dramatic within the basolateral subdivision, the target of the recordings considered in our

195   study. Other parts of amygdala like the central nucleus, by contrast, are more similar across

196   primates and rodents and it is possible that timescales could be more conserved in these nuclei.

197   Why this difference in basolateral timescales exists between the species is unknown, but work

198   by Nougaret et al. reported gradients of timescales within the basal ganglia, a circuit with well-

199   defined input and output structure (Nougaret et al., 2021). This then suggests that an area's

200   outputs might contribute to determining its timescale. Thus it follows that the basolateral

201   amygdala, which primarily projects to frontal cortex, might have longer timescales than central

202   nucleus, which primarily projects to brainstem and hypothalamus (Ghashghaei et al., 2007).

203   Future experimental work and analyses could intentionally characterize neurons from separate

204   amygdala subdivisions to determine whether anatomical and functional organization might also

205   extend to differences in timescales.

206   The macaque amygdala has a higher glia to neuron ratio, more sparse distribution of

207   neurons, and greater density of neuropil compared to rats (Chareyron et al., 2011). This

208   difference is even more stark when comparing to humans, where neurons in amygdala are even

209   more sparsely distributed than in macaques. Chareyron and colleagues speculate that these

210   specifications predispose the primate amygdala to a preferential role in integrating information

211   coming from a dramatically expanded cortex compared to rats. The basal and lateral nuclei

212   receive much of the input from the cortex and send intra-amygdala projections to other nuclei

213   (Freese and Amaral, 2009), placing them in a key position to perform such an integrative role. In

214   sensory areas, short timescales are hypothesized to be critical to quickly process and update

215   incoming information. Such shorter timescales in amygdala in humans and macaques compared

216   to mice could therefore predispose neurons in these species to be able to quickly integrate

217   information from the cortex which would in return enable the amygdala to drive learning in

218   areas with longer timescales, such as ACC (Stolyarova et al., 2019). That the primate amygdala

219   serves a more integrative role is further supported by recent insights about the organization of

220   projections from this area. Specifically, basolateral amygdala neurons in macaques exhibit

221   highly-organized patterns of collateral projections to the frontal lobe (Zeisler et al., 2023), while

222   those in mouse amygdala project more broadly in a less specific fashion (Zeisler et al., 2024).

223   While technically challenging, comparing the timescale of individual neurons whose anatomical

224   connections are known could bring important insight in our understanding of how neuronal

225   branching is related to temporal dynamics.

226   Finally, the cross-species variability in amygdala timescales stands in stark contrast to

227   hippocampus, where timescales were shorter than other brain areas measured here and highly

228   similar across species. The hippocampus exhibits much less differentiation across mammalian

229   species (Manns and Eichenbaum, 2006), with little about its anatomy and possibly the

230   computation it subserves changing throughout the course of evolution (Clark and Squire, 2013).

231   Thus, our finding that hippocampal timescales are similar across species appears to correlate

232   with such conservation. It's also striking that hippocampus had such short timescales given that

233   previous reports refer to primary sensory cortices as the prototype of an area with a short

234   timescale (Murray et al., 2014; Manea et al., 2022). Perhaps such similarity is driven by the fact

235   that most hippocampal inputs arise from the entorhinal cortex (Witter et al., 2000), in the same

236 way that primary sensory cortex inputs are predominantly from their respective sensory

237 organs.

Anatomy, granularity, commonality

239   It remains unclear what exactly about a brain area or a neuron sets its intrinsic

240 timescale. Possible contributing factors include region-wide variation in receptor expression,

241 genetic identity, intrinsic recurrence, or inputs from distant areas (Cavanagh et al., 2020;

242 Froudist-Walsh et al., 2021; Rapan et al., 2023). Indeed, we identified differences across

243 monkey cytoarchitectonic ventral frontal subdivisions (**Figure 3**). Such variation could also be

244 more significantly driven by network connectivity. Carmichael and Price have described two

245 largely non-overlapping networks within these regions (Carmichael and Price, 1996): the orbital

246 or so-called sensory network, and the medial or viscero-motor network. Recent functional

247 connectivity work (Stoll and Rudebeck, 2024b) has also explored information flow between

248 these regions and revealed that both areas 13m and 13l lack strong functional connectivity with

249 other OFC subregions during this particular decision-making paradigm. This low intra-frontal

250 connectivity might be influencing the relatively low timescale in these two subdivisions of area

251 13. By contrast, Stoll and Rudebeck show that the nearby area 12o is very highly interconnected

252 with other prefrontal regions; 12o is also more likely to receive information from many other

253 areas than to send it (Stoll and Rudebeck, 2024b). These results suggest that the highly

254 integrative role of area 12o might contribute to its relatively long timescale. Further evidence

255 for this relationship between connectivity and timescale could come from future experiments

256 targeting the visual system, with its well-documented organization of feed-forward and

257 feedback connections (Vanni et al., 2020), as one would expect shorter timescales in earlier

258 visual areas like V1 and longer timescales further up the visual hierarchy in V4 or parietal

259 cortex.

260   Within OFC, we identified spatial gradients of timescale that could not be accounted for

261 by cortical granularity alone (**Figure 3**). Rather, we found that timescales varied in a patchy

262 organization, with no clear pattern along a single anatomical axis. What drives this variation is

263 unclear, although it could be related to the projections coming into the ventral frontal cortex.

264   Inputs from the amygdala and hippocampus exhibit a sparse distribution in ventral frontal

265   cortex (Aggleton et al., 2015). Hippocampal inputs to OFC preferentially target more medial and

266   posterior areas, while amygdala inputs project more strongly to lateral areas (Ghashghaei et al.,

267   2007). Perhaps this difference in long-range innervation could drive differences in timescale

268   across the ventral surface of macaques. Within this view, the short timescale of hippocampal

269   neurons might entrain the neurons to which they project, although we note that the precise

270   effect of the presynaptic neurons' timescale on its downstream targets has yet to be assessed.

271   While often overlooked in analyses of timescales, we found that the presence or

272   absence of granule cells in layer IV modulated the latency of the exponential decay (**Figure 3B**).

273   Prior work by Fontanier, Sarazin and colleagues found that timescale and latency tend to vary

274   together and biophysical modeling revealed that the latency of a particular neuron was closely

275   related to potassium and other cationic currents (Fontanier et al., 2022). By contrast, we found

276   that variation in latency was related to granularity across macaque ventral frontal cortex,

277   whereas such a relationship was not present for timescale. Such a difference supports the idea

278   that the latency measure is distinct from timescale. Indeed, while there is consensus that a

279   longer timescale indicates a longer time interval over which a neuron might integrate

280   information (Soltani et al., 2021), a functional role for latency remains to be described. Further

281   work both *in vivo* and *in silico* is needed to fully understand how variations in latency might

282   alter computation.

283   Our analyses revealed a diversity of within-area timescales that were in some cases

284   consistent across species (**Figure 2**). The extent of these within-area differences has not been

285   previously reported. Such heterogeneity is hypothesized to be important for optimal

286   functioning both in brains and in artificial neural networks (Cavanagh et al., 2020; Stern et al.,

287   2023). Artificial neural network (ANN) modelling of prefrontal activity during a working memory

288   task suggests that timescale diversity is an adaptation to facilitate task performance; the

289   network had a largely homogenous timescale distribution before training which widened

290   significantly after repeated training iterations. Using brain-inspired spiking ANNs, Perez-Nieves

291   and colleagues successfully determined that heterogeneity is a feature of brain that is critical to

292   enable problem-solving (Perez-Nieves et al., 2021). ANN modeling therefore highlights the

293   computational significance of diverse timescales as well as the need for such heterogeneity to

294   both accurately model the brain during task performance.

295   While the timescales of neurons varied within an area we found that they were not

296   uniform but often exhibited a bimodal distribution (**Figure 2**). Importantly, a recent analysis of

297   intrinsic timescales in the macaque frontal eye field (FEF; Soyuhos et al., 2024), an area critical

298   for directing attention and coordinating eye movements, also identified bimodal distributions

299   of timescales. By characterizing these two populations using their functional properties during a

300   passive viewing task, they reported that short timescale FEF neurons primarily processed rapid

301   visual features of the task, while long timescale FEF neurons were related to sustaining

302   attention. Although a bimodal distribution was not directly reported, other studies have also

303   identified a relationship between variation in timescale and functional properties (Cavanagh et

304   al., 2020; Spitmaan et al., 2020; Fontanier et al., 2022). Since we did not characterize the

305   functional properties of the neurons included in our analysis, it remains an open question

306   whether bimodality in other brain areas is driven by related features. Further, while nearly all

307   timescale distributions considered in this analysis were bimodal, some species had uniquely

308   unimodal distributions: for example, macaque OFC or human amygdala. Whether this effect is a

309   result of the precise areas sampled or the task performed by subjects, understanding to what

310   extent bimodal distributions of timescales are ubiquitous across brain areas and behaviors is an

311   exciting next direction both for neuroscience and for computational modeling. Future research

312   should strive to further elucidate how the structure of variation of within-area timescales

313   across the cortex and subcortical structures contributes to the computational roles of those

314   areas in behavior.

315   Taken together, our data show that there are consistent timescale and latency

316   hierarchies across three commonly utilized model species: humans, macaque monkeys, and

317   mice. While we were able to reveal clear differences, particularly in OFC and amygdala, the high

318   degree of consistency across species suggests that a hierarchy of timescales might be a broad

319   organizing principle of mammalian brains. The implementation of such principles in neural

320   networks could provide improved sensitivity to both short- and long- term variation in

321   environmental inputs.

Methods:

322

323   Analyses were performed using MATLAB R2021a (MathWorks) and Python 3.9. All

324 figures made in Python used Seaborn (Waskom, 2021) and Matplotlib (Hunter, 2007) packages.

325 Other specific packages used will be cited in the methods below. Analysis code is available on

326 GitHub: https://github.com/RudebeckLab/timescales.

327   **Neurophysiological datasets**

328   Here, we analyzed the activity of single neurons recorded in humans, macaques and

329 mice across both open-source and unpublished datasets. **Table 1** illustrates the sources,

330 primary authors, and web links to these datasets as well as the papers in which they were

331 originally presented, if applicable. Unpublished datasets are indicated as such.

332   **Table 1. Datasets used for cross-species analysis.**

First Author	Species	Brain areas	# single neurons	Number of subjects	Analysis Paper Link	Dataset link
Chandra-vadia (Chandravadia et al., 2020)	Human	Amygdala Hippocampus	1086 759	59	https://doi.org/10.1038/s41597-020-0415-9	https://doi.org/10.17605/OSF.IO/HV7JA
Minxha (Minxha et al., 2020)	Human	Amygdala ACC Hippocampus	460 329 203	13	https://doi.org/10.1126/science.aba3313	https://osf.io/u3kcp/

Aquino (Aquino et al., 2024)	Human	OFC	320	9	https://doi.org/10.1523/JNEUROSCI.1628-23.2024	https://osf.io/5rv8f/
Fontanier (Fontanier et al., 2022)	Macaque	ACC	298	2	https://doi.org/10.7554/eLife.63795	https://doi.org/10.5281/zenodo.3947745
Stoll (Stoll and Rudebeck, 2024a)	Macaque	Amygdala OFC ACC	1691 5230 343	2	https://doi.org/10.1016/j.neuron.2024.03.020	Unpublished
Wirth (Wirth et al., 2017)	Macaque	Hippocampus	290	2	https://doi.org/10.1371/journal.pbio.2001045	http://crcns.org/datasets/hc/hc-12/about-hc-11
Young/ Mosher (Young et al., 2023)	Macaque	Amygdala mPFC	229 230	2	https://doi.org/10.1016/j.neuron.2023.07.012	https://zenodo.org/records/8164440
Steinmetz (Steinmetz et al., 2019)	Mouse	ACC Amygdala Hippocampus	841 317 2745	9	https://doi.org/10.1038/s4	https://figshare.com/articles/dataset/Dataset_fro

		mPFC OFC	1274 813		1586-019- 1787-x	m_Steinmet z_et_al_201 9/9598406

333

Operational Definitions of Brain Regions

335   For the sake of clearer comparisons, both within and across species, we combined
336 recordings into larger brain regions.

337   From mice (Steinmetz et al., 2019), hippocampal subfields CA1, CA2, and Dentate Gyrus
338 were all combined into the hippocampus category; Anterior cingulate area (ACA) was assigned
339 to ACC; Basolateral amygdala (BLA) to amygdala; Infralimbic area (ILA) and prelimbic cortex (PL)
340 to the mPFC category (Wise, 2008; Wallis et al., 2017); Orbital cortex (ORB) to OFC.

341   From macaque monkeys, amygdala recordings primarily targeted BLA, though precise
342 anatomical placement within amygdala was not formally assessed; OFC recordings were taken
343 from Brodmann's areas 11 and 13; subcallosal ACC (Walker's area 25) was assigned to the
344 mPFC category (Wise, 2008; Wallis et al., 2017); hippocampal recordings (Wirth et al., 2017)
345 were taken from across the extent of the hippocampus both in the antero-posterior and medio-
346 lateral planes; mid-cingulate cortex (MCC) recordings (Fontanier et al., 2022; Stoll and
347 Rudebeck, 2024a) were assigned to the ACC category, as this area has been referred both as
348 anterior MCC or dorsal ACC (Procyk et al., 2016).

349   From humans (Chandravadia et al., 2020; Minxha et al., 2020; Aquino et al., 2024), all
350 recordings were performed during seizure monitoring in cases of drug-resistant epilepsy;
351 recording targets were exclusively chosen according to clinical criteria. Amygdala recordings
352 preferentially targeted the BLA; ACC recordings were from Brodmann areas 24 and 32;
353 hippocampal recordings covered the extent of the hippocampus both in the A/P and M/L
354 planes; OFC recordings were taken primarily from Brodmann's areas 14, 13, and 10.

355   **Macaque ventral frontal cortex dataset**

356   Neural recordings were collected from two male rhesus macaques performing one of

357   two behavioral tasks: either an instrumental preference task described in Stoll and Rudebeck

358   (Stoll and Rudebeck, 2024a), or a learning task in which animals associated novel visual stimuli

359   with different reward probabilities which changed over the course of the session (unpublished).

360   Recording procedures are described in more detail in Stoll and Rudebeck (Stoll and

361   Rudebeck, 2024a). Briefly, animals were implanted with 157-channel semi-chronic recording

362   microdrives (Gray Matter Research). During recordings, animals were seated in primate chairs

363   while electrophysiological signals were recorded using the Plexon Omniplex system. Putative

364   single neurons were determined using MountainSort (Chung et al., 2017) and manually curated

365   based on cluster isolation metrics.

366   Electrodes were moved each day, and their cumulative adjustments tallied to determine

367   their precise location in the brain. CT images collected throughout the recordings and

368   histological assessment after perfusion were also used to verify these locations. Specifically,

369   following standard perfusion with 4% formaldehyde (Electron Microscopy Sciences) in

370   phosphate-buffered saline (PBS, Fisher), brains were extracted and post-fixed for 24-48 hours.

371   Brains were then cryoprotected in increasing sucrose solutions (10%, 20%, 30% sucrose in PBS)

372   before being shipped to FD NeuroTechnologies, Inc for processing, the details of which are also

373   described in detail(Stoll and Rudebeck, 2024b). Brains were further cryoprotected, frozen in

374   isopentane, and sectioned at 50um on a sliding microtome. Then equally spaced series of

375   sections were prepared for either Nissl staining (one series) or immunohistochemistry (three

376   series). Immunohistochemistry was performed for calbindin and SMI-32 in order to delineate

377   boundaries between cortical areas.

378   Boundaries between cortical areas were determined according to features described

379   previously (Carmichael and Price, 1994; Rapan et al., 2023; Stoll and Rudebeck, 2024b). In the

380   most anterior sections, areas 11m/l, 12m, and 12r were separated primarily based on SMI-32

381   staining (11m and 11l were not consistently distinguishable in these animals and so have been

382   left grouped together). 11m/l is denser with cells than the more medial 13b, and it is denser

383   with superficial neurites in layer II/III than the more lateral 12m. Then, in Nissl-stained sections,

384   the 12r and 12m can be separated based on the dysgranular layer IV in the former compared to

385   the fully granular later IV in the latter. More posteriorly, area 13l was distinguished from 13m

386   by the presence of vertical processes in calbindin-stained sections, particularly in layers III and

387   V. Area 12o was defined by its stark lack of neurite staining in SMI-32-labeled sections

388   compared to the more medial 13m. 12l was distinguished from 12o by significantly increased

389   density of SMI-32-labeled cells. Finally, agranular insular areas were distinguished from area 13l

390   on the medial side and 12o on the lateral by the distinct lack of a granular layer IV; instead,

391   significant vertical processes were observed alongside a dense and thick layer IV in SMI-32-

392   stained sections.

393   **Timescale estimation using inter-spike interval-based approach**

394   Single-neuron timescales were estimated using an inter-spike interval-based (ISI)

395   method (Fontanier et al., 2022). Fitting was performed using MATLAB 2021a. Briefly, the time

396   difference between every spike in a neuron's time series and its following 100 spikes was

397   calculated. The lagged differences were then binned at 3.33ms from 0 to 1000ms. This

398   distribution was smoothed, after which we fitted the following equation:

$$R(k\Delta) = A\left[e^{-\left(\frac{k\Delta}{\tau}\right)} + B\right]$$

400   where $k\Delta$ is the time lag between bins, τ represents the neuron's *timescale*, describing

401   the rate of decay of the autocorrelation distribution, and A and B are free parameters which

402   together describe the peak and asymptotic limit of the autocorrelation. We also extracted the

403   time bin at which the autocorrelation begins decreasing, which we refer to as *latency*. As

404   before, fitting was performed using only the decreasing portion of the autocorrelation

405   distribution (after the latency).

406   Post-processing and plotting was performed in Python 3.9 using the following packages:

407   NumPy, Pandas, Matplotlib, Seaborn, SciPy, and statsmodels. Only neurons for which the model

408 fit well ($R^2 > 0.5$) and exhibiting timescales within the range $10 < \tau < 1000$ were included for

409 further analysis. To assess the effects of species and brain region on neuronal timescales and

410 latencies, we first used an ordinary least squares regression (OLS; statsmodels *ols* function). We

411 fitted the following linear model to describe a neuron's timescale and latency in terms of the

412 species and brain region from which it was recorded:

413
$$\tau = a + b_1 * species + b_2 * brain\ region$$

414 Post-hoc tests were performed within brain regions to compare species directly with FDR

415 corrections for multiple comparisons. Timescale and latency distributions within each brain

416 area were compared using a Brown-Forsythe test for equality of variances.

417 **Firing rate analyses**

418 To ensure our timescale and latency estimates were distinct from differences in other

419 firing rate statistics, we calculated the following measures for each neuron:

- Number of spikes (*n spikes*): number of spikes in timeseries
- Mean firing rate (*mean FR*): number of spikes divided by total length of timeseries
- Normalized FR (*norm FR*): spikes were binned at 500ms, and averaged with a sliding window of 1 second (2 bins); this firing rate was then z-scored using the mean firing rate above
- Fano: *norm FR* divided by the variance of *norm FR*
- Proportion of bursts (*prop burst*): proportion of spikes included in a burst, defined as the top 0.5 percentile of the ISI distribution(Ko et al., 2012)
- Proportion of pause (*prop pause*): proportion of spikes included in a pause, defined as the bottom 0.5 percentile of the ISI distribution(Ko et al., 2012)

431 All parameters were z-scored within each species and brain region. Then, we performed

432 OLS regressions predicting both timescale and latency using each z-scored parameter

433 individually alongside species and brain region. We extracted the percent explained variance for

434   each parameter and computed p-values for each. Models were directly compared using ANOVA

435   (statsmodels *anova_lm*).

436   **Analysis of single neuron timescales in macaque ventral frontal cortex**

437   To understand whether timescales were influenced by cortical granularity, we analyzed

438   an extended dataset containing single unit activity recorded from multiple subdivisions of the

439   ventral frontal cortex in monkeys, including the previously defined OFC neurons (**Table 2**) (Stoll

440   and Rudebeck, 2024b). We then used hierarchical model comparison to determine the relative

441   contributions of both cortical granularity and area. For both timescale and latency, two OLS

442   model were built, using either the specific area or the granularity as predictors. We then

443   compared the fit of those models using *anova_lm* to determine whether the differences in

444   degrees of freedom resulted in a better fit. Neurons' position in 3D space were also computed

445   using the recording depth, MRI and CT scans as well as using histological confirmation. This

446   allowed us to assess the relationship between spatial position and timescale/latency. 3D

447   coordinates were projected into 2D space; because our AP and DV coordinates were highly

448   correlated with one another (more posterior neurons are more ventral), we focused our

449   analyses only on the A/P and M/L planes. OLS regression models were built to explain the

450   extracted timescales and latencies using the AP and ML coordinates (including the interaction

451   term).

452   **Table 2. Data used for within-frontal cortex analysis**

Cytoarchitectonic Area	Larger Brain Region	Granularity	# single neurons
11m/l	OFC (orbitofrontal cortex)	Fully granular	2199
12m	vlPFC (ventrolateral prefrontal cortex)	Fully granular	770
12l	vlPFC	Fully granular	1115

12o	vlPFC	Fully granular	2268
12r	vlPFC	Dysgranular	774
13m	OFC	Dysgranular	1425
13l	OFC	Dysgranular	1606
AI (agranular insula)	n/a	Agranular	1886

453 Neurons located in areas 11m/l, 13m, and 13l comprise the OFC category used in the cross-

454 species analysis.

Supplemental figures
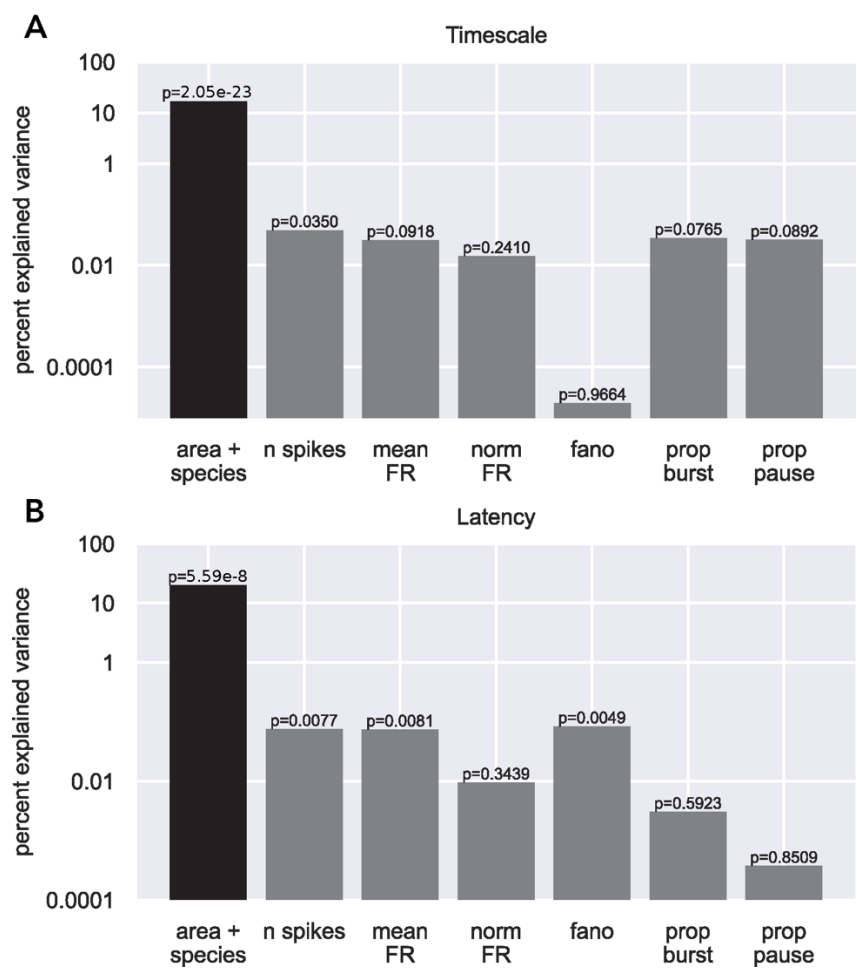
Supplemental Figure 1. Latency and timescale are weakly related to spiking statistics.

A) Percent explained variance (log scale) of timescale using a linear model containing area and species (black), and additional variance explained when including each firing rate statistic (grey). While the number of spikes was a significant predictor of timescale, the variance explained by this parameter was nearly two orders of magnitude less than the variance explained by area and species. P-values are also shown for each predictor.

B) Same as A for latency. Again, while the number of spikes, mean firing rate, and Fano factor were significant predictors of latency, together, they explain less than 1% of the total variance in latency.

References

Aggleton JP, Wright NF, Rosene DL, Saunders RC (2015) Complementary Patterns of Direct Amygdala and Hippocampal Projections to the Macaque Prefrontal Cortex. Cereb Cortex 25:4351–4373.

Aquino TG, Courellis H, Mamelak AN, Rutishauser U, O'Doherty JP (2024) Encoding of Predictive Associations in Human Prefrontal and Medial Temporal Neurons During Pavlovian Appetitive Conditioning. J Neurosci 44 Available at: https://www-jneurosci-org.us1.proxy.openathens.net/content/44/17/e1628232024 [Accessed July 5, 2024].

Carmichael ST, Price JL (1994) Architectonic subdivision of the orbital and medial prefrontal cortex in the macaque monkey. Journal of Comparative Neurology 346:366–402.

Carmichael ST, Price JL (1996) Connectional networks within the orbital and medial prefrontal cortex of macaque monkeys. Journal of Comparative Neurology 371:179–207.

Cavada C, Compañy T, Tejedor J, Cruz-Rizzolo RJ, Reinoso-Suárez F (2000) The Anatomical Connections of the Macaque Monkey Orbitofrontal Cortex. A Review. Cerebral Cortex 10:220–242.

Cavanagh SE, Hunt LT, Kennerley SW (2020) A Diversity of Intrinsic Timescales Underlie Neural Computations. Front Neural Circuits 14 Available at: https://www.frontiersin.org/articles/10.3389/fncir.2020.615626/full?utm_source=S-TWT&utm_medium=SNET&utm_campaign=ECO_FNINS_XXXXXXXX_auto-dlvrit [Accessed January 4, 2021].

Chandravadia N, Liang D, Schjetnan AGP, Carlson A, Faraut M, Chung JM, Reed CM, Dichter B, Maoz U, Kalia SK, Valiante TA, Mamelak AN, Rutishauser U (2020) A NWB-based dataset and processing pipeline of human single-neuron activity during a declarative memory task. Scientific Data 7:78.

Chareyron LJ, Lavenex PB, Amaral DG, Lavenex P (2011) Stereological analysis of the rat and monkey amygdala. Journal of Comparative Neurology 519:3218–3239.

Chung JE, Magland JF, Barnett AH, Tolosa VM, Tooker AC, Lee KY, Shah KG, Felix SH, Frank LM, Greengard LF (2017) A Fully Automated Approach to Spike Sorting. Neuron 95:1381-1394.e6.

Clark RE, Squire LR (2013) Similarity in form and function of the hippocampus in rodents, monkeys, and humans. Proc Natl Acad Sci U S A 110:10365–10370.

Fontanier V, Sarazin M, Stoll FM, Delord B, Procyk E (2022) Inhibitory Control of Frontal Metastability Sets the Temporal Signature of Cognition Behrens TE, ed. eLife 11:e63795.

499 Freese JL, Amaral DG (2009) Neuroanatomy of the primate amygdala. In: The human amygdala,
500   pp 3–42. New York, NY, US: The Guilford Press.

501 Froudist-Walsh S, Xu T, Niu M, Rapan L, Margulies DS, Zilles K, Wang X-J, Palomero-Gallagher N
502   (2021) Gradients of receptor expression in the macaque cortex. Neuroscience. Available
503   at: http://biorxiv.org/lookup/doi/10.1101/2021.02.22.432173 [Accessed April 15, 2021].

504 Gao R, van den Brink RL, Pfeffer T, Voytek B (2020) Neuronal timescales are functionally
505   dynamic and shaped by cortical microarchitecture Vinck M, Colgin LL, Womelsdorf T,
506   eds. eLife 9:e61277.

507 Ghashghaei HT, Hilgetag CC, Barbas H (2007) Sequence of information processing for emotions
508   based on the anatomic dialogue between prefrontal cortex and amygdala. NeuroImage
509   34:905–923.

510 Hasson U, Yang E, Vallines I, Heeger DJ, Rubin N (2008) A Hierarchy of Temporal Receptive
511   Windows in Human Cortex. J Neurosci 28:2539–2550.

512 Hintiryan H et al. (2021) Connectivity characterization of the mouse basolateral amygdalar
513   complex. Nat Commun 12:2859.

514 Honey CJ, Thesen T, Donner TH, Silbert LJ, Carlson CE, Devinsky O, Doyle WK, Rubin N, Heeger
515   DJ, Hasson U (2012) Slow Cortical Dynamics and the Accumulation of Information over
516   Long Timescales. Neuron 76:423–434.

517 Hubel DH, Wiesel TN (1962) Receptive fields, binocular interaction and functional architecture
518   in the cat's visual cortex. The Journal of Physiology 160:106–154.

519 Hunter JD (2007) Matplotlib: A 2D Graphics Environment. Computing in Science & Engineering
520   9:90–95.

521 Ko D, Wilson CJ, Lobb CJ, Paladini CA (2012) Detection of bursts and pauses in spike trains.
522   Journal of Neuroscience Methods 211:145–158.

523 Li S, Wang X-J (2022) Hierarchical timescales in the neocortex: Mathematical mechanism and
524   biological insights. Proceedings of the National Academy of Sciences 119:e2110274119.

525 Manea AM, Zilverstand A, Ugurbil K, Heilbronner S, Zimmermann J (2022) Intrinsic timescales as
526   an organizational principle of neural processing across the whole rhesus macaque brain
527   Lee D, ed. eLife 11:e75540.

528 Manea AMG, Maisson DJ-N, Voloh B, Zilverstand A, Hayden B, Zimmermann J (2024) Neural
529   timescales reflect behavioral demands in freely moving rhesus macaques. Nat Commun
530   15:2151.

531 Manns JR, Eichenbaum H (2006) Evolution of declarative memory. Hippocampus 16:795–808.

532 Minxha J, Adolphs R, Fusi S, Mamelak AN, Rutishauser U (2020) Flexible recruitment of
533   memory-based choice representations by the human medial frontal cortex. Science 368
534   Available at: https://science.sciencemag.org/content/368/6498/eaba3313 [Accessed
535   September 9, 2020].

536 Murray JD, Bernacchia A, Freedman DJ, Romo R, Wallis JD, Cai X, Padoa-Schioppa C, Pasternak
537   T, Seo H, Lee D, Wang X-J (2014) A hierarchy of intrinsic timescales across primate
538   cortex. Nature Neuroscience 17:1661–1663.

539 Nougaret S, Fascianelli V, Ravel S, Genovesio A (2021) Intrinsic timescales across the basal
540   ganglia. Sci Rep 11:21395.

541 Perez-Nieves N, Leung VCH, Dragotti PL, Goodman DFM (2021) Neural heterogeneity promotes
542   robust learning. Nat Commun 12:5791.

543 Procyk E, Wilson CRE, Stoll FM, Faraut MCM, Petrides M, Amiez C (2016) Midcingulate Motor
544   Map and Feedback Detection: Converging Data from Humans and Monkeys. Cerebral
545   Cortex 26:467–476.

546 Rapan L, Froudist-Walsh S, Niu M, Xu T, Zhao L, Funck T, Wang X-J, Amunts K, Palomero-
547   Gallagher N (2023) Cytoarchitectonic, receptor distribution and functional connectivity
548   analyses of the macaque frontal lobe Badre D, Baker CI, Thiebaut de Schotten M, eds.
549   eLife 12:e82850.

550 Raut RV, Snyder AZ, Raichle ME (2020) Hierarchical dynamics as a macroscopic organizing
551   principle of the human brain. PNAS 117:20890–20897.

552 Soltani A, Murray JD, Seo H, Lee D (2021) Timescales of cognition in the brain. Current Opinion
553   in Behavioral Sciences 41:30–37.

554 Soyuhos O, Moore T, Chaudhuri R, Chen X (2024) Posterior Parietal Cortex Regulates Intrinsic
555   Neural Timescales and Attentional Processing in Frontal Eye Field. :2024.09.30.615928
556   Available at: https://www.biorxiv.org/content/10.1101/2024.09.30.615928v1 [Accessed
557   October 9, 2024].

558 Spillmann L (2014) Receptive Fields of Visual Neurons: The Early Years. Perception 43:1145–
559   1176.

560 Spitmaan M, Seo H, Lee D, Soltani A (2020) Multiple timescales of neural dynamics and
561   integration of task-relevant signals across cortex. PNAS 117:22522–22531.

562 Steinmetz NA, Zatka-Haas P, Carandini M, Harris KD (2019) Distributed coding of choice, action
563   and engagement across the mouse brain. Nature 576:266–273.

564   Stern M, Istrate N, Mazzucato L (2023) A reservoir of timescales emerges in recurrent circuits
565   with heterogeneous neural assemblies Ostojic S, Frank MJ, Schwalger T, eds. eLife
566   12:e86552.

567   Stoll FM, Rudebeck PH (2024a) Preferences reveal dissociable encoding across prefrontal-limbic
568   circuits. Neuron 112:2241-2256.e8.

569   Stoll FM, Rudebeck PH (2024b) Decision-making shapes dynamic inter-areal communication
570   within macaque ventral frontal cortex. Current Biology 34:4526-4538.e5.

571   Stoll FM, Rudebeck PH (2024c) Dissociable Representations of Decision Variables within
572   Subdivisions of the Macaque Orbital and Ventrolateral Frontal Cortex. J Neurosci 44
573   Available at: https://www.jneurosci.org/content/44/35/e0464242024 [Accessed
574   October 28, 2024].

575   Stolyarova A, Rakhshan M, Hart EE, O'Dell TJ, Peters M a. K, Lau H, Soltani A, Izquierdo A (2019)
576   Contributions of anterior cingulate cortex and basolateral amygdala to decision
577   confidence and learning under uncertainty. Nat Commun 10:4704.

578   van Heukelum S, Mars RB, Guthrie M, Buitelaar JK, Beckmann CF, Tiesinga PHE, Vogt BA,
579   Glennon JC, Havenith MN (2020) Where is Cingulate Cortex? A Cross-Species View.
580   Trends in Neurosciences 43:285–299.

581   Vanni S, Hokkanen H, Werner F, Angelucci A (2020) Anatomy and Physiology of Macaque Visual
582   Cortical Areas V1, V2, and V5/MT: Bases for Biologically Realistic Models. Cereb Cortex
583   30:3483–3517.

584   Viswanathan P, Nieder A (2017) Comparison of visual receptive fields in the dorsolateral
585   prefrontal cortex and ventral intraparietal area in macaques. European Journal of
586   Neuroscience 46:2702–2712.

587   Wallis CU, Cardinal RN, Alexander L, Roberts AC, Clarke HF (2017) Opposing roles of primate
588   areas 25 and 32 and their putative rodent homologs in the regulation of negative
589   emotion. PNAS 114:E4075–E4084.

590   Waskom ML (2021) seaborn: statistical data visualization. Journal of Open Source Software
591   6:3021.

592   Wirth S, Baraduc P, Planté A, Pinède S, Duhamel J-R (2017) Gaze-informed, task-situated
593   representation of space in primate hippocampus during virtual navigation. PLOS Biology
594   15:e2001045.

595   Wise SP (2008) Forward frontal fields: phylogeny and fundamental function. Trends in
596   Neurosciences 31:599–608.

597 Witter MP, Wouterlood FG, Naber PA, Van Haeften T (2000) Anatomical Organization of the
598   Parahippocampal-Hippocampal Network. Annals of the New York Academy of Sciences
599   911:1–24.

600 Young ME, Spencer-Salmon C, Mosher C, Tamang S, Rajan K, Rudebeck PH (2023) Temporally
601   specific patterns of neural activity in interconnected corticolimbic structures during
602   reward anticipation. Neuron 111:3668-3682.e5.

603 Zeisler ZR, Heslin KA, Stoll FM, Hof PR, Clem RL, Rudebeck PH (2024) Comparative basolateral
604   amygdala connectomics reveals dissociable single-neuron projection patterns to frontal
605   cortex in macaques and mice. Current Biology 34:3249-3257.e3.

606 Zeisler ZR, London L, Janssen WG, Fredericks JM, Elorette C, Fujimoto A, Zhan H, Russ BE, Clem
607   RL, Hof PR, Stoll FM, Rudebeck PH (2023) Single basolateral amygdala neurons in
608   macaques exhibit distinct connectional motifs with frontal cortex. Neuron 111:3307-
609   3320.e5.

610